Available online at www.sciencedirect.com
SCIENCE DIRECT®
Journal of Non-Crystalline Solids 334&335 (2004) 223–227
JOURNAL OF NON-CRYSTALLINE SOLIDS
www.elsevier.com/locate/jnoncrysol

Quasicrystals in the Ti–Zr–Ni alloy system

J.B. Qiang [a], Y.M. Wang [a], D.H. Wang [a], M. Kramer [b], P. Thiel [c], C. Dong [a,c,*]

[a] State Key Lab for Materials Modification, Department of Materials Engineering, Dalian University of Technology, Dalian 116024, People's Republic of China
[b] Ames Lab, Department of Energy and Department of Materials Science and Engineering, Iowa State University, Ames, IA 50011-3020, USA
[c] Ames Lab, Department of Chemistry, Iowa State University, Ames, IA 50011-3020, USA

Abstract

The empirical compositional criteria for ternary quasicrystals (QCs) based on the QCs' phase diagram features are applied in the Ti–Zr–Ni alloy system. The ideal quasicrystals-forming composition $Ti_{40}Zr_{40}Ni_{20}$ has been identified, which lies at the crossing point of the two specific lines, termed as e/a-constant and e/a-variant lines. Bulk quasicrystalline Ti/Zr-based alloys are obtained in region of $(Ti_xZr_{100-x})_{100-y}Ni_y$ ($43.75 \leqslant x \leqslant 81.25$, $y = 17$, 20 in at.%) by copper mold casting. It was confirmed that $Ti_{40}Zr_{40}Ni_{20}$ is the optimal QC-forming composition, where a nearly pure bulk quasicrystal rod, 6 mm in diameter, can be formed. With a small deviation from this ideal composition, the Ti(Zr) solid solution phases and/or C14-type Laves phase, though as minority phases, are found coexisting with the majority icosahedral phase. At the same time, the explanation of the e/a-variant line is explored.

PACS: 61.44.Br; 81.05.Zx; 81.30.-t

1. Introduction

The Hume-Rothery mechanism plays a key role in the stabilization of quasicrystals (QCs) [1,2]. Our previous investigation on ternary Al-based quasicrystalline phase diagrams revealed that the e/a-constant and e/a-variant lines are common features in quasicrystalline systems, and the ideal composition of QCs in a given ternary system lies at the crossing point of these two lines. These lines constitute the empirical criteria to search for ideal ternary QCs compositions [3–5]. In the present work, we report a thorough structural investigation of suction-cast Ti–Zr–Ni alloys, with the aim to justify the validity of the QC formation rule in the Ti–Zr–Ni quasicrystalline system.

2. Ti–Zr–Ni phase diagram

Several Ti(Zr)-rich phases have been found in the Ti–Zr–Ni alloy system [6–12]. Their crystallographic data are collected in Table 1. Based on these results, the Ti–Zr–Ni phase diagram is drawn in Fig. 1. According to [5], the valence electron contribution of Ti, Zr, Ni can be taken as $N_{Ni} = 0$, $N_{Ti} = +1.5$, $N_{Zr} = +1.5$, then the e/a value of the Ti(Zr)-rich phases are calculated in Table 1. We can see that the e/a ratios of the known QCs and its approximants (the 1/1 W phase) are about the same and these phases are located near an e/a-constant line ($e/a = 1.20$) in the phase diagram. At the same time, we can define two e/a-variant lines by linking Ti_2Ni with the Zr corner and linking Zr_2Ni with the Ti corner. Accordingly, the ideal Ti–Zr–Ni QC composition should be located close to the crossing point of the e/a-constant and e/a-variant lines as indicated in Fig. 1.

3. Experimental

A series of Ti–Zr–Ni alloys along two e/a-constant lines ($e/a = 1.20/1.25$) with nominal compositions $(Ti_xZr_{100-x})_{100-y}Ni_y$ ($0 \leqslant x \leqslant 100$ and $y = 17$, 20 in at.% respectively) were prepared by arc-melting high-purity (>99%) Ti, Zr and Ni metals in a water-cooled copper crucible under an Ar atmosphere. The master alloys were re-melted 4 times for homogeneity. Alloy rods with 6 mm in diameter were then prepared by suction-casting

* Corresponding author. Address: State Key Lab for Materials Modification, Department of Materials Engineering, Dalian University of Technology, Dalian 116024, People's Republic of China. Tel./fax: +86-411 470 8389.
E-mail address: dong@dlut.edu.cn (C. Dong).

0022-3093/$ - see front matter © 2004 Elsevier B.V. All rights reserved.
doi:10.1016/j.jnoncrysol.2003.11.046

Table 1
Structural data of the reported Ti(Zr)-rich phases in the Ti–Zr–Ni alloy system, and the calculated e/a value of these phases

Phase	Crystallographic data/nm		Compositions (at.%)	e/a
α-(Ti,Zr)	hP2, $P6_3/mmc$	α-(Ti): $a = 0.295$, $c = 0.468$	Ti_xZr_{100-x}	1.50
		α-(Zr): $a = 0.326$, $c = 0.515$	($x = 0$–100)	
β-(Ti,Zr)	cI2, Im $\bar{3}$ m,	β-(Ti): $a = 0.3306$	Ti_xZr_{100-x}	1.50
		β-(Zr): $a = 0.3545$	($x = 0$–100)	
Ti_2Ni	cF96, Fd $\bar{3}$ m, $a = 1.1278$		$Ti_{66.7}Ni_{33.7}$	1.00
Zr_2Ni	tI12, I4/mcm, (0.6477, 0.5243)		$Zr_{66.7}Ni_{33.7}$	1.00
1/1-W phase	cI162, Im $\bar{3}$, $a = 1.4317$		$Ti_{51}Zr_{33}Ni_{16}$	1.26
			$Ti_{44}Zr_{40}Ni_{16}$	1.26
C14-TiZrNi	hP12, $P6_3/mmc$,	$a = 0.5142$–0.5191	$(Ti_{100-x}Zr_x)_2Ni$	1.00
	$MgZn_2$ type	$c = 0.8433$–0.8520	($x = 21$–30)	
B-IQC	Metastable icosahedral phase		Ti_2Ni	1.00
I phase	Low-temperature stable	$a_R = 0.512$	$Ti_{53}Zr_{27}Ni_{20}$	1.20
	Icosahedral	$a_R = 0.516$	$Ti_{45}Zr_{38}Ni_{17}$	1.25
			$Ti_{43}Zr_{40}Ni_{17}$	1.25
			$Ti_{41.5}Zr_{41.5}Ni_{17}$	1.25

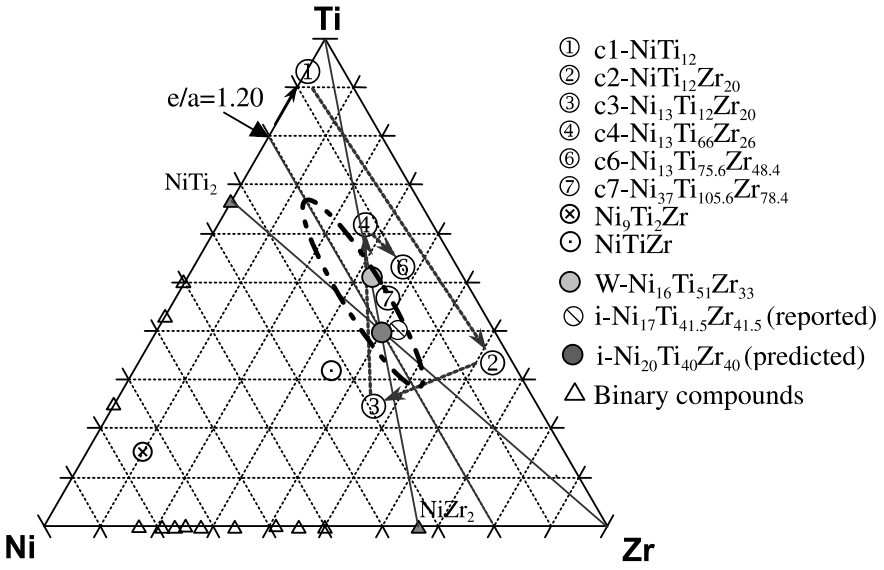

Fig. 1. Ternary phase formation section for Ti–Zr–Ni alloys (the dot–dash line shows the phase field of Ti–Zr–Ni QCs revealed by this work). The Bergman cluster of the W phase is decomposed into clusters enclosed in different shells (circled numbers). The predicted ternary i-$Ti_{40}Zr_{40}Ni_{20}$, just slightly different from reported TQC composition i-$Ti_{41.5}Zr_{41.5}Ni_{17}$, is at the crossing point of two e/a-variant lines Ti_2Ni-to-Zr and Zr_2Ni-to-Ti. The C4 and C7 clusters are located along the e/a-variant line Ti-to-TQC-to-Zr_2Ni. The dotted lines indicate the growth routes of the clusters.

of the alloy melts in a water-cooling copper mold. The structure of these as-cast samples were examined by using X-ray diffraction (XRD) with CuK_α radiation ($\lambda = 0.15406$ nm) and transmission electron microscopy (TEM). TEM specimens were prepared by standard twin-jet electrolytic thinning using an $HClO_4$–$C_2H_5O_6$ solution (volume ratio 1:8). TEM and XRD were carried out in a JEOL-100FX microscope and Shimadzu XRD-6000 diffractometer respectively.

4. Results and discussion

An XRD analysis of the as-cast rods shows that the icosahedral phase (I phase) can be formed in the composition range of $(Ti_xZr_{100-x})_{100-y}Ni_y$ ($25 \leqslant x \leqslant 87.5$, $y = 17$, 20 in at.%). In part of this range $(Ti_xZr_{100-x})_{100-y}Ni_y$ ($43.75 \leqslant x \leqslant 81.25$, $y = 17$, 20 in at.%), the I phase becomes the major phase and the minor phases are α-(Ti,Zr), β-(Ti,Zr) and C14. In the vicinity of $Ti_{40}Zr_{40}Ni_{20}$, the nearly pure quasicrystalline state can be obtained. Table 2 lists all of the XRD results of these alloys, Based on these results, the phase field of the quasicrystal was drawn in Fig. 1. Some XRD patterns of the 20 at.% Ni series alloys are shown as an example in Fig. 2; they can be mainly indexed to the I phase following the scheme of Cahn [13]. The quasilattice constant, calculated from the 20/32 peak of the quasicrystals in the 20 at.% Ni alloys, ranges from 0.5054 to 0.5259 as Zr is increased at the expense of Ti.

Table 2
Chemical and phase compositions of the Ti–Zr–Ni alloys

Composition (at.%)	Phases constitutions	Composition (at.%)	Phases constitutions
$Ti_{83}Ni_{17}$–$Zr_{83}Ni_{17}$ e/a-constant lines (e/a = 1.25)		*$Ti_{80}Ni_{20}$–$Zr_{80}Ni_{20}$ e/a-constant lines (e/a = 1.20)*	
$Zr_{83}Ni_{17}$	$\alpha + Zr_2Ni$	$Zr_{80}Ni_{20}$	$Zr_2Ni + \alpha$
$Ti_5Zr_{78}Ni_{17}$	$Zr_2Ni + \alpha$	$Ti_5Zr_{75}Ni_{20}$	$Zr_2Ni + \alpha$
$Ti_{10}Zr_{73}Ni_{17}$	$Zr_2Ni + \alpha$	$Ti_{10}Zr_{70}Ni_{20}$	$Zr_2Ni + \alpha + \beta$
$Ti_{15}Zr_{68}Ni_{17}$	$Zr_2Ni + \alpha + \beta$	$Ti_{15}Zr_{65}Ni_{20}$	$Zr_2Ni + \beta + \alpha + I$
$Ti_{20}Zr_{63}Ni_{17}$	$Zr_2Ni + \alpha + \beta$	$Ti_{20}Zr_{60}Ni_{20}$	$Zr_2Ni + I + \alpha + \beta$
$Ti_{25}Zr_{58}Ni_{17}$	$Zr_2Ni + I + \alpha + \beta$	$Ti_{25}Zr_{55}Ni_{20}$	$I + Zr_2Ni + \alpha + \beta$
$Ti_{30}Zr_{53}Ni_{17}$	$I + Zr_2Ni + \alpha + \beta$	$Ti_{30}Zr_{50}Ni_{20}$	$I + \beta + Zr_2Ni + \alpha + C14$
$Ti_{35}Zr_{48}Ni_{17}$	$I + \alpha + \beta$	$Ti_{35}Zr_{45}Ni_{20}$	$I + \alpha$
$Ti_{40}Zr_{43}Ni_{17}$	$I + \alpha$	$Ti_{40}Zr_{40}Ni_{20}$	I
$Ti_{45}Zr_{38}Ni_{17}$	$I + \alpha + C14$	$Ti_{45}Zr_{35}Ni_{20}$	$I + \alpha$
$Ti_{50}Zr_{33}Ni_{17}$	$I + \alpha + C14$	$Ti_{50}Zr_{30}Ni_{20}$	$I + \alpha$
$Ti_{55}Zr_{28}Ni_{17}$	$I + \alpha$	$Ti_{55}Zr_{25}Ni_{20}$	$I + \alpha$
$Ti_{60}Zr_{23}Ni_{17}$	$I + \alpha$	$Ti_{60}Zr_{20}Ni_{20}$	$I + C14 + \alpha$
$Ti_{65}Zr_{18}Ni_{17}$	$I + \alpha + C14$	$Ti_{65}Zr_{15}Ni_{20}$	$I + \alpha + C14$
$Ti_{70}Zr_{13}Ni_{17}$	$I + \alpha + C14$	$Ti_{70}Zr_{10}Ni_{20}$	$Ti_2Ni + \alpha + I$
$Ti_{75}Zr_8Ni_{17}$	$\alpha + Ti_2Ni$	$Ti_{75}Zr_5Ni_{20}$	$\alpha + Ti_2Ni$
$Ti_{83}Ni_{17}$	$\alpha + Ti_2Ni$	$Ti_{80}Ni_{20}$	$\alpha + Ti_2Ni$

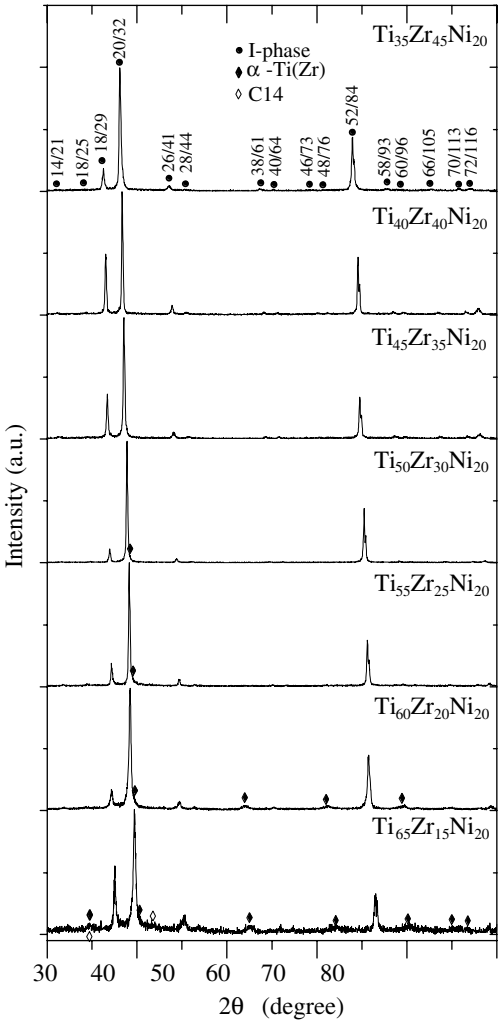

Fig. 2. XRD patterns of the as-cast Ti–Zr–Ni quasicrystalline rods with 20 at.% Ni.

As-cast quasicrystalline rods from these alloys have a smooth surface and good luster, and are pore-free; Fig. 3 shows their outer shape and surface appearance. The quasicrystalline nature of the QC rods are also confirmed by TEM examination. Selected area electron diffraction (SAED) patterns and a bright-field TEM image (BF image) of the I-$Ti_{40}Zr_{40}Ni_{20}$ phase are shown in Fig. 4. The I phase, having a primitive lattice, manifests phason-free diffraction features. The grain size is a few μm in diameter, and the bright-field morphology of the QCs, shown in Fig. 4, have an interesting speckled contrast that does not change much when tilted in the electron microscope; this is similar to features for the Ti–Fe–Si I phase [14]. As shown in Figs. 5 and 6, with a small deviation from the ideal composition $Ti_{40}Zr_{40}Ni_{20}$, the Ti(Zr) solid solution phases and/or the C14-type Laves phase are found coexisting with the majority I phase. In the Ti-rich quasicrystalline alloys, the Ti(Zr) solid solution always has the form of α-Ti(Zr) (hP2) (Fig. 5(a)), while the β-Ti(Zr) (cI2) is formed in the

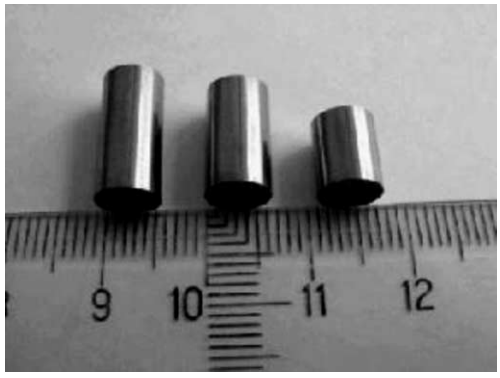

Fig. 3. Outer surface appearance of as-cast Ti–Zr–Ni quasicrystalline rods showing the smooth surface and good luster.

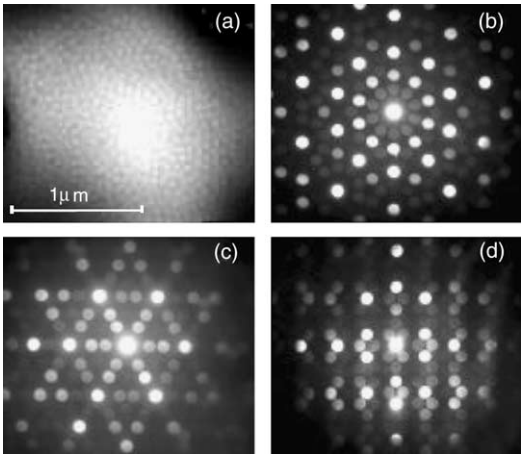

Fig. 4. Typical bright-field (BF) image and selected area electron diffraction (SAED) patterns of the as-cast $Ti_{40}Zr_{40}Ni_{20}$ bulk quasicrystal, (a) BF image, (b) 5-fold, (c) 3-fold, (d) 2-fold.

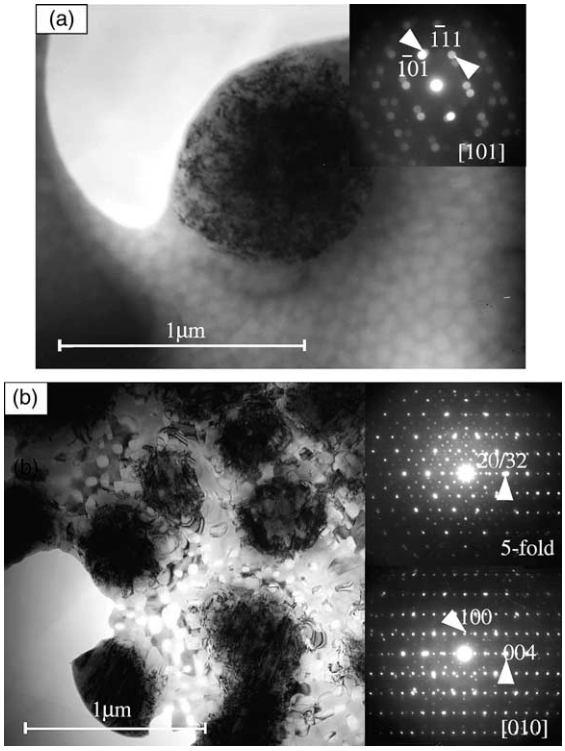

Fig. 5. The BF image and SAED patterns of the as-cast $Ti_{65}Zr_{15}Ni_{20}$ alloy, (a) α-Ti(Zr)(dark gray) + I phase, (b) C14 (black) + I phase.

Zr-rich quasicrystalline alloys (Fig. 6). The β-Ti(Zr) always has an orientation relationship to the icosahedral phase: $\langle 0\,0\,1\rangle_\beta // \langle 1, 3\tau+1, \tau\rangle_I$, $\{1\,1\,0\}_\beta // \{18/29\}_I$ (Fig. 6). And there also exists a orientation relationship between C14-TiZrNi and the icosahedral phase: $\langle 0\,1\,0\rangle_{C14} // \langle 5\text{-fold}\rangle_I$, $\{0\,0\,4\}_{C14} // \{20/32\}_I$ (Fig. 5(b)).

As shown in Fig. 1, both the e/a-constant and e/a-variant lines exist in the Ti–Zr–Ni phase diagram. We note first that a linear QC composition zone extends

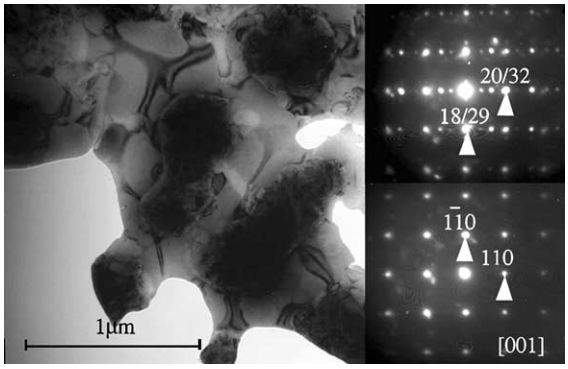

Fig. 6. The BF image and SAED patterns of the as-cast $Ti_{30}Zr_{50}Ni_{20}$ alloy.

along the e/a-constant lines ($e/a = 1.20$–1.25), showing typical e/a-constant phase phenomenon. On the other hand, the two e/a-variant lines defined by linking Ti_2Ni to Zr and Zr_2Ni to Ti, exactly cross with the e/a-constant line ($e/a = 1.20$) at the composition of $Ti_{40}Zr_{40}Ni_{20}$, the optimal QC-forming composition, where a nearly pure quasicrystalline state can be fabricated directly by conventional casting. This is also in good agreement with reported composition of $Ti_{41.5}Zr_{41.5}Ni_{17}$ [6]. So the QC formation rule based on the e/a-constant and e/a-variant lines is still valid for Ti–Zr–Ni QCs.

While the e/a-constant phenomenon is known to be related to the stabilization mechanism involving Fermi sphere–Brillouin zone interaction [15,16], the e/a-variant line deserves further explanation. In the following, we take the Zr_2Ni–Ti e/a-variant line as an example to clarify the structural relationship of the phases for this kind of specific line.

The Ti–Zr–Ni ternary quasicrystal (TQC) phase is of the Bergman type and is related to the Bergman phase W-$Ti_{51}Zr_{33}Ni_{16}$, which is the 1/1-approximant of QCs [17]. According to the above mentioned composition rules, the possible TQC should be located at $Ti_{40}Zr_{40}Ni_{20}$, the crossing point of two e/a-variant lines Ti_2Ni-to-Zr and Zr_2Ni-to-Ti, because the Ti_2Ni-type structure (Zr_2Ni can also show this type of structure under rapid cooling condition [18]) is the approximant of the Ti-based binary QCs [19,20]. Note that the W and QC phases are both on the specific e/a-variant line Ti-to-Zr_2Ni. Since the fcc-Zr_2Ni phase (Ti_2Ni type) is also based on the Bergman cluster [20], all of the phases along this line, except the pure element Ti, are based on the Bergman cluster. In order to further clarify this point, the Bergman cluster in the W phase is decomposed into a shelled structure going from the center to the outer shells one finds a central Ni atom, a 1st-shell icosahedron (12 Ti atoms, i.e. 12Ti), a 2nd-shell dodecahedron (20Zr), a 3rd-shell icosahedron (12Ni), a 4th-shell truncated icosahedron (54Ti6Zr), a 5th-shell

dodecahedron (4.8Ti–15.2Zr), a 6th-shell icosahedron (4.8Ti–7.2Zr), and a 7th-shell complex polyhedron (24Ni–30Ti–30Zr). In Fig. 1, the clusters enclosed by different shells are indicated in the Ti–Zr–Ni-ternary phase diagram. We note that the cluster that encompasses everything up to the 4th shell ('C4') is located exactly on the e/a-variant line of Ti-to-Zr_2Ni, together with the Bergman phase and the TQC i-$Ti_{40}Zr_{40}Ni_{20}$. The growth from the C4 to the Bergman phase and eventually to the TQC can then be regarded as a mixing of C4 clusters with a glue structure whose composition is Zr_2Ni. The proportion of these two structures is C4:$Zr_2Ni = 4.27:1$ in W-$Ti_{51}Zr_{33}Ni_{16}$, and C4:$Zr_2Ni = 1.75:1$ in i-$Ti_{40}Zr_{40}Ni_{20}$. The structural feature defining the other e/a-variant line between Zr and Ti_2Ni is not yet clear. Since the fcc Ti_2Ni phase is based on the Bergman cluster, we suspect that this line is also based on Bergman clusters, but with different chemical stoichiometries from those on the Ti-to-Zr_2Ni line. Therefore, the e/a-variant line is related to the growth mode of a certain basic cluster; in general, it is defined by linking all the phases constructed from the same basic cluster. In the Ni–Ti–Zr system, the $NiZr_2$-to-Ti e/a-variant line is based on the same C4 cluster.

5. Conclusion

In general, in ternary quasicrystalline alloy systems, there exist both e/a-constant and e/a-variant lines. The former suggests that QCs and approximants are e/a-constant phases belonging to a group of Hume-Rothery phases with similar e/a ratios. The latter one indicates that ternary QCs and binary ones are closely related by common building blocks. The ideal composition of the ternary QCs lies at the crossing point of the e/a-constant and e/a-variant lines. By applying this rule we reveal that a broad bulk-quasicrystal-forming region, $(Ti_xZr_{100-x})_{100-y}Ni_y$ ($43.75 \leqslant x \leqslant 81.25$, $y = 17$, 20 in at.%), has been identified in the Ti–Zr–Ni system. Among them, $Ti_{40}Zr_{40}Ni_{20}$ is the optimal composition, where a nearly pure bulk quasicrystal sample can be obtained. With a small deviation from the ideal composition, the α- and β-Ti(Zr) solid solution phases and/or C14-type Laves phase are found coexisting with the majority I phase, though as minority phases.

Acknowledgements

Supported by Natural Science Foundation of China (59971014).

References

[1] S.J. Poon, Adv. Phys. 41 (1992) 303.
[2] Z.M. Stadnik (Ed.), Physical Properties of Quasicrystals, Springer, Berlin, Germany, 1999.
[3] J.B. Qiang, Y.M. Wang, W.R. Chen, C. Dong, J. Mater. Res., Sin. 16 (2002) 500 (in Chinese).
[4] J.B. Qiang, D.H. Wang, C.M. Bao, Y.M. Wang, W.P. Xu, M.L. Song, C. Dong, J. Mater. Res. 16 (2001) 2653.
[5] Y.M. Wang, J.B. Qiang, C.H. Wong, C.H. Shek, C. Dong, J. Mater. Res. 18 (2003) 642.
[6] K.F. Kelton, W.J. Kim, R.M. Stroud, Appl. Phys. Lett. 70 (1997) 3230.
[7] A. Sibirtsev, V.N. Chebotnikov, V.V. Molokanov, Y.K. Kovneristyi, TETP Lett. 47 (1988) 744.
[8] V.V. Molokanov, V.N. Chebotnikov, J. Non-Cryst. Solids 117&118 (1990) 789.
[9] R.M. Stroud, K.F. Kelton, S.T. Misture, J. Mater. Res. 12 (1997) 434.
[10] W.J. Kim, P.C. Gibbons, K.F. Kelton, Philos. Mag. Lett. 76 (1997) 199.
[11] W.J. Kim, P.C. Gibbons, K.F. Kelton, W.B. Yelon, Phys. Rev. B 58 (1998) 2578.
[12] J.P. Davis, E.H. Majzoub, J.M. Simmons, K.F. Kelton, Mater. Sci. Eng. A 294–296 (2000) 104.
[13] J.W. Cahn, D. Shechtman, D. Gratias, J. Mater. Res. 1 (1986) 13.
[14] P. Mandal, R.S. Tiwari, O.N. Srivastava, Philos. Mag. A 63 (1991) 617.
[15] C. Dong, L.M. Zhang, Brunet, E. Belin-Ferre, J.M. Dubois, Mater. Sci. Eng. A 304–306 (2001) 172.
[16] C. Dong, Scr. Metall. Mater. 33 (1995) 239.
[17] R.G. Hennig, E.H. Majzoub, A.E. Carlsson, K.F. Kelton, C.L. Henley, W.B. Yelon, S. Misture, Mater. Sci. Eng. A 294–296 (2000) 361.
[18] Z. Altounian, E. Batalla, J.O. Strom-Olsen, J.L. Walter, J. Appl. Phys. 61 (1987) 149.
[19] Q.B. Yang, K.H. Kuo, Acta Crystallogr. A 52 (1987) 787.
[20] Q.B. Yang, Philos. Mag. B 61 (1990) 155.